Biol Chem. 2009; 390(2): 181-9
Published online 2007 March 8. Doi: http://dx.doi.org/10.1515/BC.2009.017

BiologicalChemistry'JustAccepted'Papers

Biological Chemistry 'Just Accepted' Papers are papers published online, in advance of appearing in the print journal. They have been peer-reviewed, accepted and are online published in manuscript form, but have not been copy edited, typeset, or proofread. Copy editing may lead to small differences between the *Just Accepted* version and the final version. There may also be differences in the quality of the graphics. When papers do appear in print, they will be removed from this feature and grouped with other papers in an issue.

Biol Chem 'Just Accepted' Papers are citable; the online publication date is indicated on the Table of Contents page, and the article's Digital Object Identifier (DOI), a unique identifier for intellectual property in the digital environment (e.g., 10.1515/BC.2007.052), is shown at the top margin of the title page. Once an article is published as ***Biol Chem 'Just Accepted' Paper*** (and before it is published in its final form), it should be cited in other articles as follows:

> Kusuhara, K., Madsen, K., Jensen, L., Hellsten, Y. and Pilegaard, H., **Calcium signaling in regulating PGC-1α, PDK4 and HKII mRNA expression**. Biol Chem, electronic publication on March 8, 2007, DOI 10.1515/BC.2007.052.

After a paper is published in ***Biol Chem 'Just Accepted' Paper*** form, it proceeds through the normal production process, which includes copy editing, typesetting and proofreading. The edited paper is then published in its final form in a regular print and online issue of ***Biol Chem.*** At this time, the ***Biol Chem 'Just Accepted' Paper*** version is replaced on the journal Web site by the final version of the paper with the same DOI as the ***Biol Chem 'Just Accepted' Paper*** version.

Disclaimer

Biol Chem 'Just Accepted' Papers have undergone the complete peer-review process. However, none of the additional editorial preparation, which includes copy editing, typesetting and proofreading, has been performed. Therefore, there may be errors in articles published as ***Biol Chem 'Just Accepted' Papers*** that will be corrected in the final print and online version of the Journal. Any use of these articles is subject to the explicit understanding that the papers have not yet gone through the full quality control process prior to advanced publication.

Biological Chemistry 'Just Accepted' paper = ISSN (online) 1437-4315
D O I: 10.1515/BC.2009.017

Isotope tracing enhancement of chemiluminescence assays for nitric oxide research

Julia Cornelius[1,a], Tuan Tran[1,a], Nicole Turner[1,a], Abigail Piazza[1,a], Lauren Mills[1,a], Ryan Slack[1,a], Sean Hauser[1], J. Steven Alexander[2], Matthew B. Grisham[2], Martin Feelisch[3] and Juan Rodriguez[1,2,*]

[1]Centenary College of Louisiana, Department of Physics, Shreveport, LA 71134, USA
[2]Louisiana State University Health Sciences Center, Department of Molecular and Cellular Physiology, Shreveport, LA 71130, USA
[3]Clinical Sciences Research Institute, Warwick Medical School, University of Warwick, Coventry CV4 7AL, UK

*Corresponding author
e-mail: jrodrigu@centenary.edu

[a]These authors contributed equally to this work.

Abstract

Chemiluminescence assays are used widely for the detection of nitric oxide (NO)-derived species in biological fluids and tissues. Here we demonstrate that these assays can be interfaced with mass-sensitive detectors for parallel determination of isotopic abundance. Results obtained with tri-iodide and ascorbic acid-based reductive assays indicate that mass spectrometric detection enables NO isotope-tracing experiments to be carried out to a limit of detectability of a few picomol, a sensitivity similar to that of standard gas phase chemiluminescence methods. The advantage afforded by mass spectrometric detection is demonstrated using the murine macrophage cell line J774, which is shown here to reduce $^{15}NO_3^-$ to $^{15}NO_2^-$ under anoxic conditions. The particular combination of an analytical and cellular system described here may hold promise for future characterization of the enzymatic pathways contributing to mammalian nitrate reductase activity, without background interference from $^{14}NO_2^-$ derived from other sources.

Keywords: chemiluminescence assay; isotope tracing; mass spectrometer; nitrate; nitrate reductase; nitric oxide, nitrite.

Introduction

Nitric oxide (NO) plays an important role in cell signaling by promoting a wide range of posttranslational protein modifications, such as heme nitrosylation and S-nitrosation. Despite the attention that these signaling mechanisms have received in the last two decades, there remains much ambiguity about the precise chemical pathways that link NO sources to the resulting protein modifications. For instance, the classical NO-signaling pathway involving heme-nitrosylation, which includes the prototypical activation of soluble guanylyl cyclase, is widely viewed as arising from capture of NO generated from local enzymatic NO synthesis via oxidation of L-arginine. It is now recognized that nitrite (NO_2^-) may also contribute to hemeprotein nitrosylation via interaction with the mitochondrial electron transport chain (Walters et al., 1967; Nohl et al.; 2000, Tischner et al., 2004), deoxyhemoglobin (Cosby et al., 2003: Hunter et al., 2004), myoglobin (Rassaf et al., 2007; Shiva et al., 2007; Hendgen-Cotta et al., 2008), xanthine oxidase (Li et al., 2004; Webb et al., 2004), non-enzymatic formation of NO as a result of disproportionation of nitrous acid (Zweier et al., 1995; Hunter et al., 2004), and a co-operative mechanism between hemes and thiols (Bryan et al., 2005). In the case of protein S-nitrosation, the process can potentially occur through many intermediate pathways that involve reactions with higher order nitrogen oxides (e.g. N_2O_4 or N_2O_3) (Williams, 1988) superoxide (Schrammel et al., 2003), metal ions (Williams, 1988; Stubauer et al., 1999), thiyl radicals (Jourd'heuil et al., 2003) and nitrite (Bryan et al., 2005). Further compounding this

complexity, the chemical pathways connecting NO sources to potential protein modifications are critically dependent on intracellular conditions (e.g. oxygen tension, pH, redox state), on the presence of hydrophobic regions in proximity to NO sources (Liu et al., 1998), and on the nature of the protein microenvironment around the thiol group (Stamler et al., 1997; Ascenzi et al., 2000). The multiplicity of potential pathways is thus leading to a growing realization that much work remains to be done before the role NO plays in cellular function can be fully characterized. Attaining this level of understanding will require a combination of analytical tools that not only are capable of detecting biologically relevant levels of NO-related products, but also able to trace their chemical origin through isotopic differentiation.

A common approach for the detection of biologically generated NO species is the NO chemiluminescence assay. This approach relies on the extraction of NO from selective species, either chemically or optically, and their subsequent detection with an NO chemiluminescence detector where trace levels of NO are detected in the gas phase through its chemiluminescent reaction with ozone (Fontijn, 1970). When coupled to the gas efflux from purge vessels containing reducing/oxidizing solutions or from UV irradiated capillaries, this detector can quantify NO products, including nitrite and nitrate (Walters et al., 1978; Cox and Frank, 1982; Dunham et al., 1995; Yang et al., 1997; Trushina et al., 1997), nitroso products (Massey et al., 1984; Stamler et al., 1992; Samouilov and Zweier, 1998; Ewing and Janero, 1998; Gladwin et al., 2000; Rassaf et al., 2002; Jourd'heuil et al., 2005; Wang et al., 2005; Zhang et al., 2005), nitrosyl-hemes (Gladwin et al., 2000; Feelisch et al., 2002) and total NO (Sonoda et al., 1997). The wide use of NO chemiluminescence detectors in life science laboratories can be attributed to several factors, including sensitivity, selectivity, quick response, ease of use, and the relatively moderate pricing and space requirements that are comparable to other commonly used laboratory instruments. Here we describe an enhancement to NO chemiluminescence assays that retains their original advantages while providing isotopic differentiation capabilities. Following earlier work by Russow (1999) on mass spectrometric detection of NO from aqueous nitrite and nitrate using a chemical vessel, this work demonstrates that a mass spectrometer detector can either replace, or operate in parallel with, NO chemiluminescence detectors without altering assay conditions and sacrificing convenience. The approach incorporates a detector that is commonly used in GC/MS systems, which is also sold as a stand-alone system with supporting data acquisition software. Our results indicate that mass spectrometric detection used in this way allows NO isotopic-tracing experiments to be carried out to a limit of detectability of a few picomoles. The advantage afforded by mass spectrometric detection is illustrated by providing evidence that the murine macrophage J774 displays nitrate reductase capabilities, as demonstrated by the emergence of $^{15}NO_2^-$ immediately following the addition of $^{15}NO_3^-$ to cell lysates.

Results

Apparatus

The apparatus described here for the isotopic detection of NO products is shown schematically in Figure 1. The setup is based on those designed previously for the use of NO-ozone chemiluminescence detection (CLD), with a few modifications to accommodate the added mass-sensitive detector (MSD) and to control the relative flow toward both instruments. The CLD in our lab is a Dasibi 2108 (Dasibi Environmental Corp., Glendale, USA), modified to process the output from the photomultiplier tube (PMT) directly into a DAT-710 A/D converter (DataQ Instruments, Akron, OH, USA) using a sampling rate of 1 Hz. The nominal intake flow rate for this instrument is 100 ml/min and the NO sensitivity under direct PMT monitoring is approx. 10 ppb. The MSD used here (5975B XL; Agilent Technologies, CA, USA) employs electron impact ionization and a high-volume turbopump (ca. 260 l/min). The flow to the MSD is restricted by a 0.25mm ID fused silica gas chromatography (GC) column measuring 7.5 m in length, resulting in an intake flow rate of 4 ml/min for an input pressure of 2 atmospheres. The column is maintained at all times at a temperature of 100°C inside an oven (1321F; VWR, West Chester, PA, USA) to prevent accumulation of adsorbed gases that may occur primarily when the apparatus is not in use. A hole two inches in diameter was bored through the side of the oven to accommodate the MSD inlet in order to prevent condensation of volatile species at that point. The MSD is operated in selected ion monitoring (SIM) mode, scanning for masses m/z = 29, 30, and 31. Integration times were set to either 100 ms for scanning conditions using MSD auto-tuning parameters or 400 ms when operating under manually adjusted MSD parameters (see below).

Samples containing NO related products are injected into a 40 ml Sievers purge vessel (GE Analytical Instruments, Boulder, CO, USA), containing a suitable reactive solution that strips the NO off its binding site and releases it into the gas phase. The vessel is continuously purged with ultrahigh-purity helium (UHP He) with an inlet gauge pressure of typically 20-40 psi (135-270 kPa) that rapidly extracts dissolved NO from the solution and transports it at rates of 50-100 ml/min towards the detectors for quantification. Water vapor transported by the carrier gas is partially recondensed by the jacketed condenser that is built into the Sievers purge vessel, maintained here near 0°C. The remaining gas is filtered through a 10 ml Sievers purge vessel containing a 1 M solution of NaOH to trap corrosive gases and higher order nitrogen oxides. Finally, the water vapor of the gas en route to the detectors is reduced by the condenser built into the second purge vessel, which is also maintained near 0°C.

The gas sample emerging from the chemical vessels is split by a Swagelok T connector between the two detectors. The majority of the flow (>90%) is directed toward the CLD since the MSD flow is limited to 4 ml. To help maintain the intake pressure near 1 atm for the CLD,

the line leading to it is opened to the atmosphere with the aid of a T connector that is uncapped at one end. This open point also acts as a constant pressure point that helps to regulate upstream where the flow splits toward the MSD. Exposure to atmospheric NO contributes minimally to our signals since our lab is located in a wooded campus within a relatively small metropolitan area. In areas where NO levels are higher and variable, the same pressure regulation could be achieved with the aid of a balloon attached to the open end, which is filled periodically with He. Finally, a needle valve between the two T's adjusts the flow through that line in order to control the balance of flow between the MS and CL detectors.

Even with non-detectable levels of atmospheric NO, air contamination in the gas stream can produce small contributions to the signals at m/z = 30 as demonstrated in Figure 3. The contribution at m/z=30 is likely due to the partial fragmentation of O_2 and N_2 in the ion source, followed by recombination into NO. The signal observed at m/z=31 always tracks the levels of O_2 at m/z=32 and is likely due to crosstalk between the two mass channels. Control of air leaks into the gas lines is therefore critical for proper quantification of NO with minimal interference. Since molecular oxygen can diffuse with ease through plastics, care is taken to avoid using these materials in the gas lines. Our apparatus makes use of 1/8 inch (3.2 mm) stainless steel (SS) tubing, except for a portion leading to the chromatography (GC) column which used 1/16 inch (1.8 mm) tubing. All tubing is joined with SS Swagelok connectors. Coupling of the GC column to the 1/16 inch tubing is achieved with a Valco 1/16 inch stainless steel internal union with a fused silica adapter ferrule on the column side. In addition to air tight tubing and junctions, our apparatus makes use of injection septa designed for GC injectors. Another factor that affects these levels is contamination of the lines leading to the MSD, which is particularly evident when they are opened and exposed to atmospheric gases. For this reason we typically isolate those lines at the end of the day by shutting the switch-valve and the Teflon valve at the exit of the second condenser and keeping the MSD running continuously. In addition to leaks, one must contend with dissolved air that may be present in solution. For samples that can be studied under anoxic conditions, the air contamination can be eliminated simply by purging with pure argon for 30 seconds prior to injection into the reaction vessel. Whenever experiments require extended periods of purging, e.g. biological samples that must be maintained anoxic for several minutes, it is recommended that the gas be scrubbed with NaOH to trap NOx contaminants that may result in the creation of artifactual NO-related products. When normoxic or hypoxic conditions are required, we resort to an analytical procedure that uses information obtained from m/z = 29 to subtract the contributions due to contamination at m/z = 30 and 31. This procedure is discussed below in the section.

As illustrated in Figures 1-5, signals obtained with MS detection are very similar in lineshape to those obtained with chemiluminescence (Feelisch et al., 2002). They are best described by exponentially modified gaussian functions, resulting from the convolution of gaussian

processes such as diffusion of gases, and exponentially decaying processes such as reaction kinetics in the purge vessel, extraction of the analytes from the reducing solution, and detector response. Our analysis software (Peakfit, Systat Software, CA, USA) allows for incorporation of this profile information to determine the best peak fit, underlying background, and area under the peak. Figure 2 shows a representative curve fit obtained with a 100 pmol injection of nitrite into a tri-iodide assay.

Performance under autotuned MSD operation and with minimal signal processing In this section we describe the performance of MSD based NO detection under two experimental conditions that facilitate MSD operation and minimize signal processing: autotuning MSD operation and use of He under high pressure/flow settings. Autotuning offers a hands-free approach to maintaining instrument sensitivity and selectivity. It allows a mass spectrometer to determine its own voltage and current settings that ionize and guide molecules towards their detectors. The performance is optimized for selectivity and sensitivity over a wide range of molecular masses, but not necessarily for smaller mass ranges such as the one targeted in this study. The second aforementioned experimental condition is the adoption of pressure settings that in our experience minimizes baseline fluctuations and thus facilitates subsequent signal analysis. Those were found to occur at a supply and split flow gauge pressures of 40 and 32 psi, respectively. In the next section we describe other conditions that require additional optimization and signal processing but provide greater sensitivity. Both approaches are presented separately here in the interest of those who may wish to duplicate our system for the following reasons. The first approach is easier to implement and may be sufficiently sensitive to quantify NO products in e.g. translational studies using biological fluids such as plasma and urine. Furthermore, it offers a valuable benchmark to meet before attempting to implement the more advanced changes that provide greater sensitivity.

Typical MSD tracings extracted for the signals at m/z = 29, 20, and 31 are shown in Figure 3. The curves illustrate the performance of the system obtained with 1 nmol injections of $^{14}NO_2^-$, $^{15}NO_2^-$, and of an equimolar mixture of $^{14}NO_2^-$ and $^{15}NO_2^-$, all in Ar-purged PBS. The fourth injection illustrates the signals generated by dissolved air in fully aerated buffered solutions. Large amplitude signals are seen with every injection, with ionic masses in accordance to the substances injected and to their proportions. The large peak arises from $^{14}N^{15}N$ (natural abundance of 0.73%). Smaller artifactual signals are also seen in adjacent mass channels. The smaller signal registered at m/z=31 during the first injection of $^{14}NO_2^-$ arises in part from the isotopic contribution from $^{15}N^{16}O$ and $^{14}N^{17}O$ (total natural abundance of 0.4%) with the remaining contribution (approx. 0.6%) arising from cross-talk with the m/z=30 signal. The next injection of $^{15}NO_2^-$ also displays a small signal at m/z=30 corresponding to a 2% fraction of the 1 nmol injection of $^{15}NO_2^-$. This fraction is consistent with the 2% $^{14}NO_2^-$ impurity level quoted by the $^{15}NO_2^-$ supplier. Lastly, the small signals at m/z = 30 and 31 seen with injections of a

fully aerated PBS sample arise from $^{14}N^{16}O$ formed by partial fragmentation of O_2 and N_2 in the ion source, and from crosstalk between the larger signal at m/z=32 ($^{16}O^{16}O$) and m/z=31.

To test the linearity of our MSD approach and its correlation with chemiluminescence detection, 100 µl solutions of $^{15}NO_2^-$ with concentrations of 100 nM, 300 nM, 1 µM, 3 µM and 10 µM, where injected in triplicate into an I^-/I_3^-/HCl reductive assay (see Figure 4). The top panel of Figure 4 shows a realtime scan extraction for m/z = 31 corresponding to the expected mass for ^{15}NO. The peak areas for those injections are shown in the middle panel of Figure 4 as a function of $^{15}NO_2^-$ injected. The linearity of the response is evaluated through a power law fit $y = ax^b$ and resulted in a near-unity power dependence with b=0.9733. The lower panel compares the same integrated signals with those obtained simultaneously with a chemiluminescence detector. The near-linear relationship between the two confirms that the MSD signals observed are due to the detection of NO. Similar MSD limearity and correlation with chemiluminescence detection were obtained with injections of $^{14}NO_2^-$ and monitoring of m/z 30 (data not shown).

Similar experiments were conducted with the nitrite specific reactive mixture containing ascorbic acid and HCl. Compared to the tri-iodide assay, the ascorbic acid based assay produces broader temporal signals with consequently lower limits of detection (approx. 30 pmol, see Figure 5, top panel).

Extended performance using reduced purge flow, manual tuning, and background subtraction

Additional hardware adjustments and signal processing have enabled us to achieve extended performance in terms of sensitivity and in the ability of handling aerated samples. To attain higher signals we lowered the flow rate to the chemiluminescence relative to that into the MS detector. Best results were achieved at a He supply and split-flow gauge pressures of 20 psi and 17 psi, respectively. Under these operating conditions we observe that the duration of the NO signals is increased from 0.2 to more than 0.8 minutes. Further gain in signal to noise ratio were attained with adjustments to parameters that control the performance of the MSD analyzer. One simple adjustment takes advantage of the fourfold increase in duration of the NO signals registered under lower flow conditions. This enabled us to decrease the sampling rate fourfold by increasing the integration time from 100 to 400 ms per ion. A four-fold increase in integration time resulted in a twofold increase in signal to noise ratio. Additional sensitivity was obtained with manual adjustments to default and autotuned parameters that control the MSD analyzer. Using an electron ionization current of 60.6 µA, and voltages for ion focusing, the repeller, entrance lens, and entrance lens offset of 90.2V, 30.12V, 40.0V, and 15.31V, respectively, we were able to increase the integrated signal another fourfold without significant changes in background noise.

A drawback from lower pressure operation is the emergence of ripples in the baseline with a period also on the order of a minute, as illustrated in middle panel of Figure 5. The nature of the ripple is unclear at this time since it manifests itself at only at selected m/z ions including all the ones monitored here. However, since the ripples at m/z = 30 and 31 are consistently in phase with the one at m/z=29, we followed a simple procedure that uses the data from the latter to correct for the ripple in the former ions. To null the ripple at m/z=30, for instance, the data from m/z=29 was first scaled down by a constant factor and then subtracted from the data at m/z=30. The factor selected corresponded to one that minimized the standard deviation for a portion of the subtracted curve that should normally be flat, i.e. a portion before or after the signal. The minimization of the standard deviation can be accomplished manually by trial and error or using an automatic routine such as the Solver option available in Microsoft Excel. The effectiveness of this background subtraction procedure is illustrated in the lower panel of Figure 5.

The background subtraction procedure outlined above proved effective for samples purged of air. For un-purged samples, where dissolved air produces artifacts as illustrated in Figure 3, we developed an additional procedure that subtracts the air artifacts from the signals. The relative contributions of air to the signals at m/z=29, 30 and 31 were first determined using fully aerated buffer injections and Peakfit analysis. Once these contributions were standardized, the m/z=29 trace in the samples was inspected for air signals which were analyzed with Peakfit for amplitude and shape. This information together with the scaling factors obtained with aerated standards allowed us to estimate the anticipated amplitude and shape of air contributions at m/z=30 and 31. Once those contributions were subtracted from the data in all three traces the ripple subtraction and signal analysis proceeded as outlined above.

Together, the adjustments made to the flow through the purge vessels and to the MSD analyzer increased our overall signal to noise ratio by nearly one order of magnitude. Figure 7 demonstrates the increased sensitivity achieved when all enhancements described above were implemented. The results show that signals as low as 3 picomoles could be quantified using the ascorbic acid assay. Similar performance (data not shown) was achieved using the tri-iodide based assay. Although the adjusted values quoted here are largely specific for the mass spectrometer model we use, it suggests that similar adjustments when implemented with other models could likely result in significantly enhanced performance.

Isotopic detection in J774 cells

There is currently much interest surrounding the biological activity and therapeutic uses of nitrite, an oxidative product of NO synthesis that until recently was regarded as biologically inert (Gladwin et al., 2005). The interest in this anion has been intensified further with recent evidence that mammalian tissues can reduce nitrate to nitrite through the action of xanthine oxidase (Jansson et al., 2008), an enzyme that plays a significant role in the immune system.

Since macrophages are part of that system and constitutively express this enzyme, we sought to explore whether these cells are able to reduce $^{15}NO_3^-$ (nitrate) to $^{15}NO_2^-$ (nitrite) using our mass selective technique.

A representative set of data from our mass selective experiments is shown in the top panel of Figure 7. The hatched gray zone around the horizontal axis represents our limit of detectability, i.e. the area where measurements essentially correspond to baseline fluctuations. Following J774.2 cell homogenization, samples were kept aerated at 37°C as 100 µl volumes were drawn periodically and injected into an ascorbic acid based nitrite assay. Each column in the Figure represents the average of three injections performed over a period of 20 minutes following 10 minutes of Ar purging, for a total of 30 minutes. The gray and white columns in the top panel of Figure 7 show the levels of $^{14}NO_2^-$ and $^{15}NO_2^-$, respectively, before and after addition of 100 µM $^{15}NO_3^-$ to the lysate at the 90 minute mark. The data shows the emergence of $^{15}NO_2^-$ only after addition of $^{15}NO_3^-$, consistent with the notion that J774.2 cells should exhibit nitrate reductase activity. Similar experiments performed with control culture flasks incubated without J744.2 cells, confirm that the $^{15}NO_3^-$ reduction is obtained only in the presence of cells. The lower panel of Figure 7 compares results obtained for $^{15}NO_2^-$ before and after addition of 100 µM $^{15}NO_3^-$ to lysates, for Ar-purged and un-purged samples. These results demonstrate that the nitrate reductase activity of J774 cells is potently inhibited by oxygen.

In addition to the signals obtained for $^{15}NO_2^-$, the upper panel of Figure 7 illustrates the artifactual progressive increase in the $^{14}NO_2^-$ signal usually seen when a biological sample or culture media is purged with an industrial grade gas that has not been scrubbed with NaOH. The increase was not observed in our standards or PBS alone. This phenomenon is attributed to hydrolysis of NOx species present in the purge gas, which interestingly seems to be potentiated by the presence of biological material in the sample. The ability of our system to discern isotopically nitrate-to-nitrite reduction from other reactions that produce nitrite only demonstrates the advantage of using isotopic tracing methods to characterize sources of NO signaling.

Discussion

The current work demonstrates that mass spectrometric detection can be successfully incorporated into NO chemiluminescence assays with relative ease to provide isotopic tracing capabilities. The system described here places an MS detector in parallel with an NO chemiluminescence detector mainly to validate our findings, but the MS detector could have easily been used as the sole detector in the system if desired. The limit of detection for both ^{14}NO and ^{15}NO is on the order of a few pmol using the MSD option, rendering it nearly as sensitive as chemiluminescence detection. Tests with cell homogenates indicate that these detection limits are also attainable in with biological samples.

The present technique offers advantages and imposes limitations that should be considered carefully before adopting it. The main advantage of our MS based technique is its direct compatibility with chemiluminescence based NO assays, which not only allows it to use extensively validated chemical assays but also facilitates cross-referencing of results obtained by either technique. The benchtop space requirements and the detector costs are also essentially similar for either technique. Another advantage associated with MS detectors is that their technology has matured to the point of providing turn-key operation and easy servicing steps. Consumable items such as electron impact filaments, detector horns, capillary columns, are widely available through a variety of vendors at competitive pricing. Compared to costlier and more labor-intense GC/ Negative Ion Chemical Ionization MS techniques that rely on derivatization of NO-related products (Tsikas, 2000), the current technique offers the advantage that biological samples can be assessed for nitrite, nitroso, and nitrosyl-heme species within a few minutes and with minimal sample preparation. Finally, unlike laser IR techniques reported to date which enable sensitive detection of ^{14}NO or ^{15}NO, but not both simultaneously (Gabler and Lehmann, 2005; Yi et al., 2006; Fritsch et al., 2008), our MS approach is able to cycle between those two detection channels in only a few milliseconds therefore allowing simultaneous detection of ^{14}NO and ^{15}NO with equal sensitivity. Laser-based techniques are also significantly costlier than the technique described here.

In terms of disadvantages and limitations, the lowest concentration of NO-related products that can be quantified currently with our technique is on the order of tens of nM assuming that sampling is performed in 100 µl volumes. This level of sensitivity most likely precludes its use for studies of basal nitrosation and heme nitrosylation in small animals (Bryan et al., 2004). Such products may be best studied using GC/MS (Tsikas, 2000) or one of the IR laser spectroscopic methods (Fritsch et al., 2008) alluded to above. Nevertheless the sensitivity of our technique should still be sufficient to trace isotopically other products such as nitrite and nitrate in fluids and tissues of small animals. Another disadvantage is the inconvenience imposed by the additional data processing steps required to subtract the contributions of

dissolved air from the NO signals. In the future, this inconvenience may be minimized through programmed steps using software developed in-house.

Finally, we demonstrated the applicability of the present technique with experiments focused on the detection of nitrate-to-nitrite reduction in anoxic J774.2 cell lysates. When lysates were spiked with ^{15}N-labeled nitrate, we observed very clearly its reduction to ^{15}N-nitrite, even as the levels of $^{14}NO_2^-$ changed due to other processes. Our analytical system also enabled us to determine that the reduction of nitrate to nitrite was distinctly suppressed in aerated samples. These results suggest that this cellular model combined with our analytical system may hold promise for future characterization of the enzymatic pathways contributing to mammalian nitrate reductase activity.

Materials and methods

Standard solutions of $^{14}NO_2^-$ and $^{15}NO_2^-$ were prepared from $Na^{14}NO_2$ and $Na^{15}NO_2$ (Sigma-Aldrich, St. Louis, MO, USA) in 40 mM HEPES or phosphate-buffered saline (PBS) solutions. All samples were bubbled with argon (Ar) for 30 seconds prior to injection to remove dissolved air, which produces some interference at m/z = 30 and 31. They were then injected in 100µL volumes into a 40 mL Sievers reaction vessel containing either tri-iodide (Feelisch et al., 2002) or ascorbic acid based solutions (Nagababu and Rifkind, 2007), in which 1 M HCl was substituted for acetic acid to avoid background interference from the molecular fragments CH_2OH at m/z = 31(NIST). The tri-iodide solution consisted of 1M HCl at room temperature, to which 10 mg of I_2 and 300 mg of KI were added. The ascorbic acid solution was prepared from a mixture of 32 ml of 1 M HCl and 4 ml of 0.5 M ascorbic acid maintained at 37°C. The nitrite specificity of the ascorbic acid/HCl mixture was validated with side by side injections of nitrite, nitrate, and S-nitrosoglutathione (Sigma-Aldrich). The NO formed from the reduction of nitrite was purged out of the reaction vessel with ultrahigh-purity helium (UHP He) and scrubbed through a 1 M NaOH solution, and quantified with our combined CLD/MS detection system described in the following section.

J774.2 cells (Sigma-Aldrich) were grown to near confluence (5-7 days) in T75 flasks with DMEM in the presence of 10% fetal bovine serum (Sigma-Aldrich), penicillin (200 U/ml), and streptomycin (200 µg/ml). On the day of the experiment, the cell culture supernatant was aspirated and the adherent cells were washed 2-3 times with sterile PBS. Cells were then collected by scraping using a rubber policeman into 1-2 ml of PBS and lysed using an Ar-pressurized Parr Bomb. The resulting cell lysate was used immediately in experiments. Control flasks were incubated under identical conditions for the same period of time without cells and processed identically to those containing cells. In addition, the media from each of the control flasks were centrifuged in 15 ml tubes, at 1000 *g* for 60 minutes. The remaining pellet was re-

suspended in 1 ml of PBS and tested immediately.

Acknowledgments

His work was supported through grants from the Louisiana Biomedical Research Network (National Institutes of Health Award No. 2 P20 RR016456) and the National Science Foundation (Award No. 0641516).

References

Ascenzi, P., Colasanti, M., Persichini, T., Muolo, M., Polticelli, F., Venturini, G., Bordo, D. and Bolognesi, M. (2000). Re-evaluation of amino acid sequence and structural consensus rules for cysteine-nitric oxide reactivity. Biol. Chem. *381*, 623-627.

Bryan, N. S., Fernandez, B. O., Bauer, S. M., Garcia-Saura, M. F., Milson, A. B., Rassaf, T., Maloney, R. E., Bharti, A., Rodriguez, J. R. and Feelisch, M. (2005). Nitrite is a signaling molecule and a regulator of gene expression in mammalian tissues. Nat. Chem. Biol. *1*, 290-297.

Bryan, N. S., Rassaf, T., Maloney, R. E., Rodriguez, C. M., Saijo, F., Rodriguez, J. R. and Feelisch, M. (2004). Cellular targets and mechanisms of nitros(yl)ation: an insight into their nature and kinetics *in vivo*. Proc. Natl. Acad. Sci. USA *101*, 4308-4313.

Cosby, K., Partovi, K. S., Crawford, J. H., Patel, R. K., Reiter, C. D., Martyr, S., Yang, B. K., Waclawiw, M. A., Zalos, G., Xu, X., et al. (2003). Nitrite reduction to nitric oxide by deoxyhemoglobin vasodilates the human circulation. Nat. Med. *9*, 1498-1505.

Cox, R. D. and Frank, C. W. (1982). Determination of nitrate and nitrite in blood and urine by chemiluminescence. J. Anal. Toxicol. *6*, 148-152.

Dunham, A. J., Barkley, R. M. and Sievers, R. E. (1995). Aqueous nitrite ion determination by selective reduction and gas phase nitric oxide chemiluminescence. Anal. Chem. *67*, 220-224.

Ewing, J. F. and Janero, D. R. (1998). Specific S-nitrosothiol (thionitrite) quantification as solution nitrite after vanadium(III) reduction and ozone-chemiluminescent detection. Free Radic. Biol. Med. *25*, 621-628.

Feelisch, M., Rassaf, T., Mnaimneh, S., Singh, N., Bryan, N. S., Jourd'Heuil, D. and Kelm, M. (2002). Concomitant S-, N-, and heme-nitros(yl)ation in biological tissues and fluids: implications for the fate of NO *in vivo*. FASEB J. *16*, 1775-1785.

Fontijn, A., Sabadell, A. J., and Ronco, R. J. (1970). Homogeneous chemiluminescent measurement of nitric oxide with ozone. Anal. Chem. *42*, 575-579.

Fritsch, T., Brouzos, P., Heinrich, K., Kelm, M., Rassaf, T., Hering, P., Kleinbongard, P. and

Murtz, M. (2008). NO detection in biological samples: differentiation of ^{14}NO and ^{15}NO using infrared laser spectroscopy. Nitric Oxide *19*, 50-56.

Gabler, R. and Lehmann, J. (2005). Sensitive and isotope selective ($^{14}NO/^{15}NO$) online detection of nitric oxide by faraday-laser magnetic resonance spectroscopy. Methods Enzymol. *396*, 54-60.

Gladwin, M. T., Ognibene, F. P., Pannell, L. K., Nichols, J. S., Pease-Fye, M. E., Shelhamer, J. H. and Schechter, A. N. (2000). Relative role of heme nitrosylation and β-cysteine 93 nitrosation in the transport and metabolism of nitric oxide by hemoglobin in the human circulation. Proc. Natl. Acad. Sci. USA *97*, 9943-9948.

Gladwin, M. T., Schechter, A. N., Kim-Shapiro, D. B., Patel, R. P., Hogg, N., Shiva, S., Cannon, R. O., 3rd, Kelm, M., Wink, D. A., Espey, M. G., et al. (2005). The emerging biology of the nitrite anion. Nat. Chem. Biol. *1*, 308-314.

Hendgen-Cotta, U. B., Merx, M. W., Shiva, S., Schmitz, J., Becher, S., Klare, J. P., Steinhoff, H. J., Goedecke, A., Schrader, J., Gladwin, M. T., et al. (2008). Nitrite reductase activity of myoglobin regulates respiration and cellular viability in myocardial ischemia-reperfusion injury. Proc. Natl. Acad. Sci. USA *105*, 10256-10261.

Hunter, C. J., Dejam, A., Blood, A. B., Shields, H., Kim-Shapiro, D. B., Machado, R., Tarekegn, S., Mulla, N., Hopper, A. O., Schechter, A. N., et al. (2004). Inhaled nebulized nitrite is a hypoxia-sensitive NO-dependent selective pulmonary vasodilator. Nat. Med. *10*, 1122-1127.

Jansson, E. A., Huang, L., Malkey, R., Govoni, M., Nihlen, C., Olsson, A., Stensdotter, M., Petersson, J., Holm, L., Weitzberg, E. and Lundberg, J. O. (2008). A mammalian functional nitrate reductase that regulates nitrite and nitric oxide homeostasis. Nat. Chem. Biol. *4*, 411-417.

Jourd'heuil, D., Jourd'heuil, F. L. and Feelisch, M. (2003). Oxidation and nitrosation of thiols at low micromolar exposure to nitric oxide. Evidence for a free radical mechanism. J. Biol. Chem. *278*, 15720-15726.

Jourd'heuil, D., Jourd'heuil, F. L., Lowery, A. M., Hughes, J. and Grisham, M. B. (2005). Detection of nitrosothiols and other nitroso species *in vitro* and in cells. Methods Enzymol. *396*, 118-131.

Li, H., Samouilov, A., Liu, X. and Zweier, J. L. (2004). Characterization of the effects of oxygen on xanthine oxidase-mediated nitric oxide formation. J. Biol. Chem. *279*, 16939-16946.

Liu, X., Miller, M. J., Joshi, M. S., Thomas, D. D. and Lancaster, J. R., Jr. (1998). Accelerated reaction of nitric oxide with O_2 within the hydrophobic interior of biological membranes. Proc. Natl. Acad. Sci. USA *95*, 2175-2179.

Massey, R. C., Key, P. E., McWeeny, D. J. and Knowles, M. E. (1984). The application of a chemical denitrosation and chemiluminescence detection procedure for estimation of the apparent concentration of total N-nitroso compounds in foods and beverages. Food

Addit. Contam. *1*, 11-16.

Nagababu, E. and Rifkind, J. M. (2007). Measurement of plasma nitrite by chemiluminescence without interference of S-, N-nitroso and nitrated species. Free Radic. Biol. Med. *42*, 1146-1154.

NIST Standard Reference Database 69, NIST Chemistry WebBook.

Nohl, H., Staniek, K., Sobhian, B., Bahrami, S., Redl, H. and Kozlov, A. V. (2000). Mitochondria recycle nitrite back to the bioregulator nitric monoxide. Acta Biochim. Pol. *47*, 913-921.

Rassaf, T., Bryan, N. S., Kelm, M. and Feelisch, M. (2002). Concomitant presence of N-nitroso and S-nitroso proteins in human plasma. Free Radic. Biol. Med. *33*, 1590-1596.

Rassaf, T., Flogel, U., Drexhage, C., Hendgen-Cotta, U., Kelm, M. and Schrader, J. (2007). Nitrite reductase function of deoxymyoglobin: oxygen sensor and regulator of cardiac energetics and function. Circ. Res. *100*, 1749-1754.

Russow, R. (1999). Determination of ^{15}N in ^{15}N-enriched nitrite and nitrate in aqueous samples by reaction continuous flow quadrupole mass spectrometry. Rapid Commun. Mass Spectrom. *13*, 1334-1338.

Samouilov, A. and Zweier, J. L. (1998). Development of chemiluminescence-based methods for specific quantitation of nitrosylated thiols. Anal. Biochem. *258*, 322-330.

Schrammel, A., Gorren, A. C., Schmidt, K., Pfeiffer, S. and Mayer, B. (2003). S-nitrosation of glutathione by nitric oxide, peroxynitrite, and $*NO/O_2*^-$. Free Radic. Biol. Med. *34*, 1078-1088.

Shiva, S., Huang, Z., Grubina, R., Sun, J., Ringwood, L. A., MacArthur, P. H., Xu, X., Murphy, E., Darley-Usmar, V. M. and Gladwin, M. T. (2007). Deoxymyoglobin is a nitrite reductase that generates nitric oxide and regulates mitochondrial respiration. Circ. Res. *100*, 654-661.

Sonoda, M., Kobayashi, J., Takezawa, M., Miyazaki, T., Nakajima, T., Shimomura, H., Koike, K., Satomi, A., Ogino, H., Omoto, R. and Komoda, T. (1997). An assay method for nitric oxide-related compounds in whole blood. Anal. Biochem. *247*, 417-427.

Stamler, J. S., Jaraki, O., Osborne, J., Simon, D. I., Keaney, J., Vita, J., Singel, D., Valeri, C. R. and Loscalzo, J. (1992). Nitric oxide circulates in mammalian plasma primarily as an S-nitroso adduct of serum albumin. Proc. Natl. Acad. Sci. USA *89*, 7674-7677.

Stamler, J. S., Toone, E. J., Lipton, S. A. and Sucher, N. J. (1997). (S)NO signals: translocation, regulation, and a consensus motif. Neuron *18*, 691-696.

Stubauer, G., Giuffre, A. and Sarti, P. (1999). Mechanism of S-nitrosothiol formation and degradation mediated by copper ions. J. Biol. Chem. *274*, 28128-28133.

Tischner, R., Planchet, E. and Kaiser, W. M. (2004). Mitochondrial electron transport as a source for nitric oxide in the unicellular green algae *Chlorella sorokiniana*. FEBS Lett. *576*, 151-155.

Trushina, E. V., Oda, R. P., Landers, J. P. and McMurray, C. T. (1997). Determination of nitrite

and nitrate reduction by capillary ion electrophoresis. Electrophoresis *18*, 1890-1898.

Tsikas, D. (2000). Simultaneous derivatization and quantification of the nitric oxide metabolites nitrite and nitrate in biological fluids by gas chromatography/mass spectrometry. Anal. Chem. *72*, 4064-4072.

Walters, C. L., Casselden, R. J. and Taylor, A. M. (1967). Nitrite metabolism by skeletal muscle mitochondria in relation to haem pigments. Biochim. Biophys. Acta *143*, 310-318.

Walters, C. L., Downes, M. J., Hart, R. J., Perse, S. and Smith, P. L. (1978). Determination of nitrite at low level without prior extraction. Z. Lebensm. Unters. Forsch. *167*, 229-232.

Wang, J., Chan, W. G., Haut, S. A., Krauss, M. R., Izac, R. R. and Hempfling, W. P. (2005). Determination of total N-nitroso compounds by chemical denitrosation using CuCl. J. Agric. Food Chem. *53*, 4686-4691.

Webb, A., Bond, R., McLean, P., Uppal, R., Benjamin, N. and Ahluwalia, A. (2004). Reduction of nitrite to nitric oxide during ischemia protects against myocardial ischemia-reperfusion damage. Proc. Natl. Acad. Sci. USA *101*, 13683-13688.

Williams, D. L., ed. (1988). Nitrosation (Cambridge, UK: Cambridge University Press).

Yang, F., Troncy, E., Francoeur, M., Vinet, B., Vinay, P., Czaika, G. and Blaise, G. (1997). Effects of reducing reagents and temperature on conversion of nitrite and nitrate to nitric oxide and detection of NO by chemiluminescence. Clin. Chem. *43*, 657-662.

Yi, J., Namjou, K., Zahran, Z. N., McCann, P. J. and Richter-Addo, G. B. (2006). Specific detection of gaseous NO and ^{15}NO in the headspace from liquid-phase reactions involving NO-generating organic, inorganic, and biochemical samples using a mid-infrared laser. Nitric Oxide *15*, 154-162.

Zhang, Y., Keszler, A., Broniowska, K. A. and Hogg, N. (2005). Characterization and application of the biotin-switch assay for the identification of S-nitrosated proteins. Free Radic. Biol. Med. *38*, 874-881.

Zweier, J. L., Wang, P., Samouilov, A. and Kuppusamy, P. (1995). Enzyme-independent formation of nitric oxide in biological tissues. Nat. Med. *1*, 804-809.

Figure legends

Figure 1 Diagram highlighting key features of the setup for simultaneous detection of NO products using chemiluminescence and mass spectrometers detectors.

Figure 2 Analysis of a 100 pmol signal generated with MS detection.
The dots correspond to data points collected directly from the MSD, while the solid curve represents a data fit to an exponentially modified Gaussian over a linearly graded background. Curvefitting is performed with Peakfit which automatically determines optimal parameters for the peak and the background, and automatically calculates the area under the peak.

Figure 3 Typical MSD tracings extracted for the signals at m/z = 29, 30, and 31.
The curves illustrate the performance of the system obtained with 1 nmol injections of $^{14}NO_2^-$, $^{15}NO_2^-$, and of an equimolar mixture of $^{14}NO_2^-$ and $^{15}NO_2^-$, all in Ar-purged phosphate-buffered saline solution. The fourth injection illustrates the signals generated by dissolved air in fully aerated buffered solutions. The large peak arises from $^{14}N^{15}N$ (natural abundance 0.73%; see text for details).

Figure 4 $^{15}NO_2^-$ quantification using a tri-iodide assay and standard MS detection conditions (see text).
Top panel: realtime scan of multiple $^{15}NO_2^-$ injections of increasing concentration. Middle panel: areas under the curve for the injections shown in the top panel. Lower panel: comparison between the areas under the curve measured simultaneously with MS and CL detection.

Figure 5 Performance comparison between autotune/high-pressure, manual-tune/low-pressure, and manual-tune/low-pressure/signal-subtraction modes of operation.
All panels show signals obtained at m/z=30 with two injections of 30 pmol of $^{14}NO_2^-$ into an ascorbic acid/HCl assay. The upper panel shows barely discernable signals obtained with injections at 5 and 7.5 minutes under autotune/high-pressure conditions. The middle panel exemplifies the enhancement in performance that is achieved with lower pressure and MSD manual tuning. A drawback from this mode of operation is the emergence of ripple in the baseline with a period comparable to that of the signal. The lower panel demonstrates that much of the ripple can be eliminated by subtracting a fraction of the signal at m/z=29 to further enhance the sensitivity of the system.

Figure 6 Quantification of $^{14}NO_2^-$ (upper panel) and $^{15}NO_2^-$ (lower panel) using an ascorbic acid/HCl assay and enhanced MS detection conditions (see text).

Figure 7 Mass-selective detection of nitrite from the murine J774.2 macrophage cell line.

'l11e gray and white columns in the top panel show the levels of $^{14}1\backslash O_2$ and $^{15}1\backslash O_2$. respectively, before and after addition of lOOf!m of $^{15}1\backslash O_3$ to the lysate at the 90 minute mark The gray hatched zone around the horizontal axis represents our limit of dctcctability, i,c, the area where measurements are essentially indistinguishable ±!·om baseline fluctuations The lower panel compares results obtained tor $^{15}NO_2$ prim·to and after addition of 100 f!m of $^{15}1\backslash O_3$ to lysates, for i\r-purged samples (white columns) or un-purged (hatched columns),

Isotope tracting for NO chemiluminescence assays

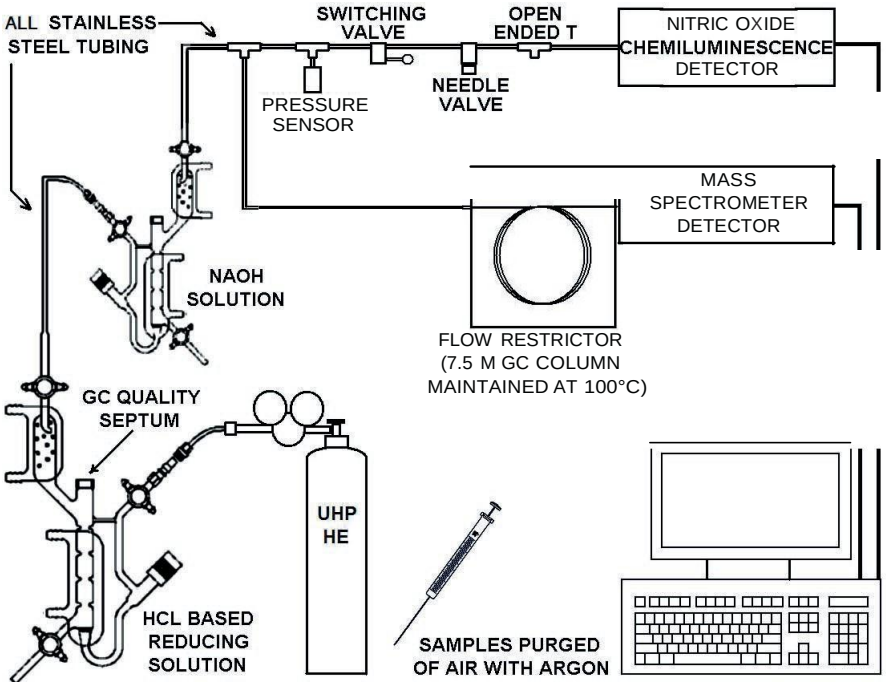

Isotope tracting for NO chemiluminescence assays

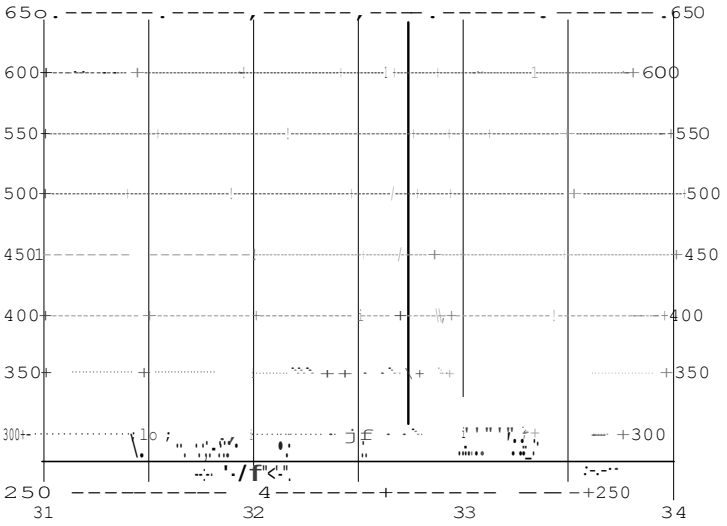

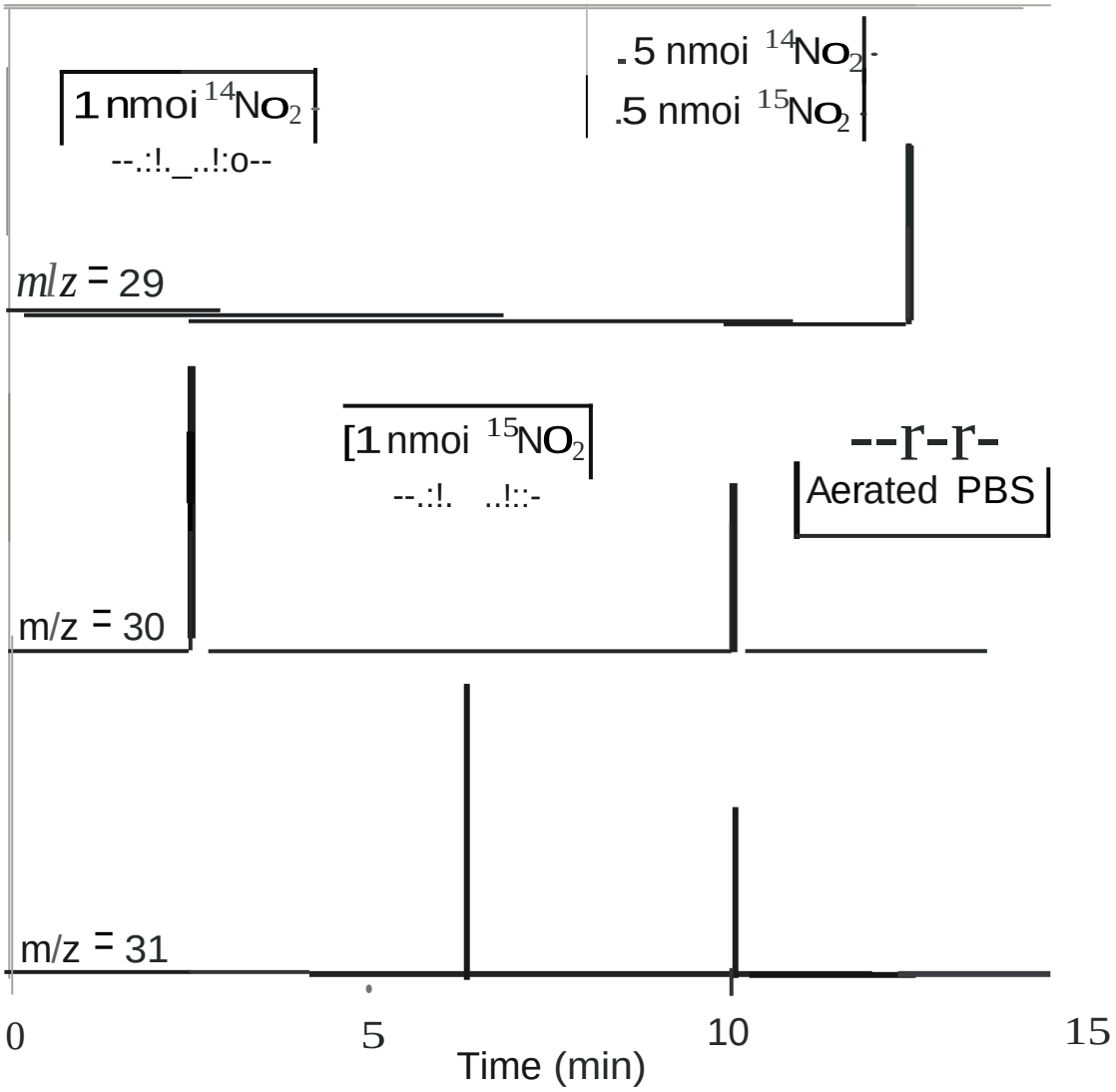
1 nmoi $^{14}NO_2$ -
.5 nmoi $^{14}NO_2$ -
.5 nmoi $^{15}NO_2$ -
m/z = 29
[1 nmoi $^{15}NO_2$
Aerated PBS
m/z = 30
m/z = 31
0
5
10
15
Time (min)

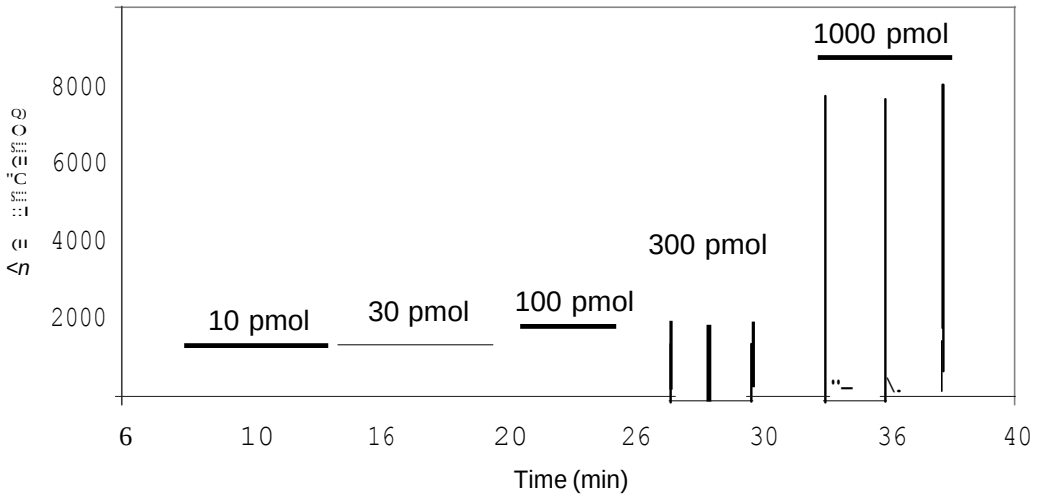
1000 pmol
8000
6000
4000
2000
300 pmol
10 pmol
30 pmol
100 pmol
6
10
16
20
26
30
36
40
Time (min)

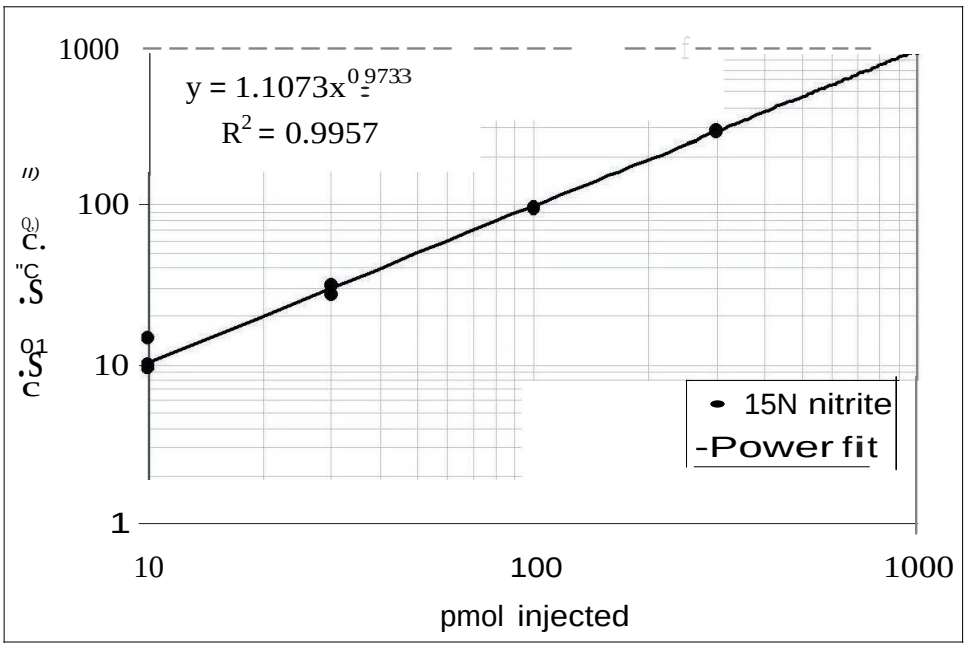
1000
y = 1.1073x^0.9733
R2 = 0.9957
100
10
1
15N nitrite
-Power fit
10
100
1000
pmol injected

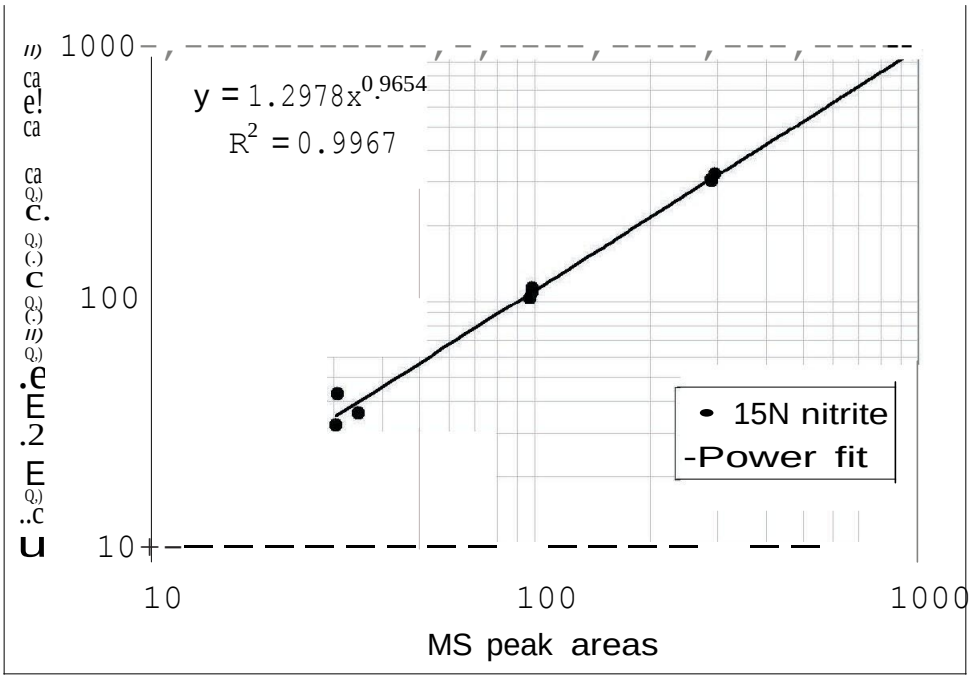
1000
y = 1.2978x^0.9654
R2 = 0.9967
100
10
15N nitrite
-Power fit
10
100
1000
MS peak areas

Isotope tracting for NO chemiluminescence assays

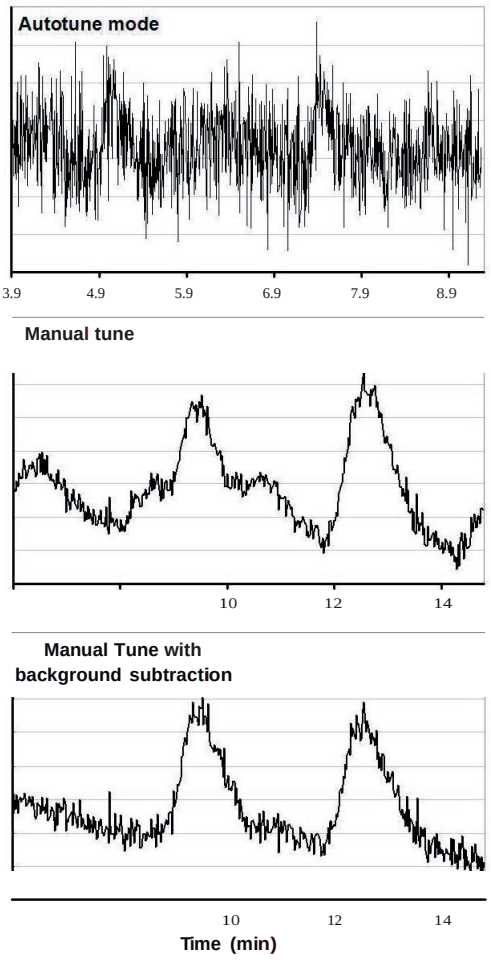

Isotope tracting for NO chemiluminescence assays

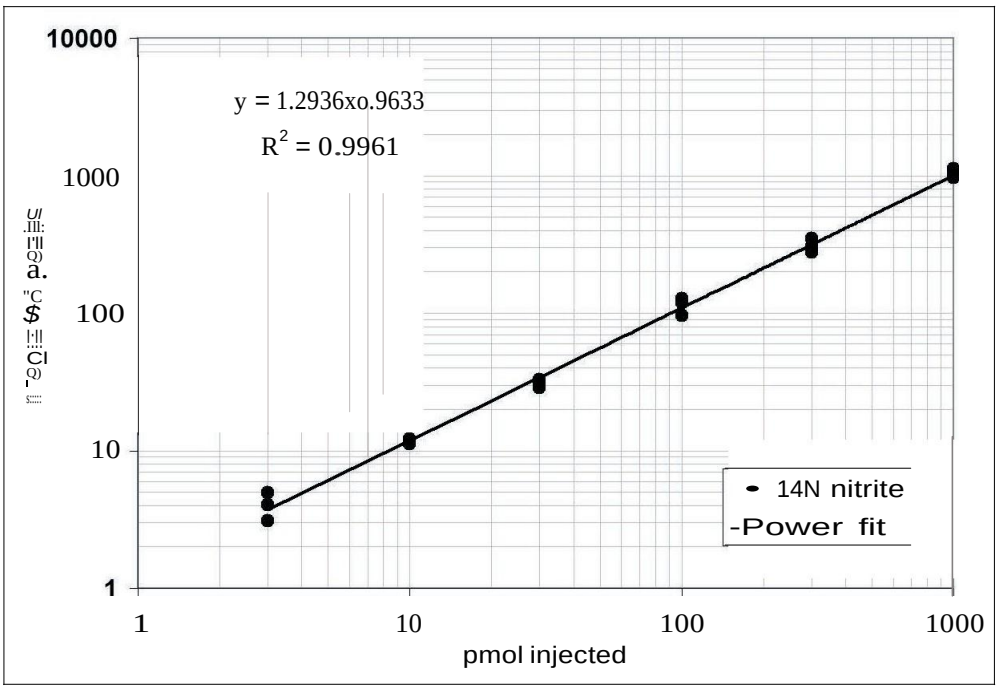

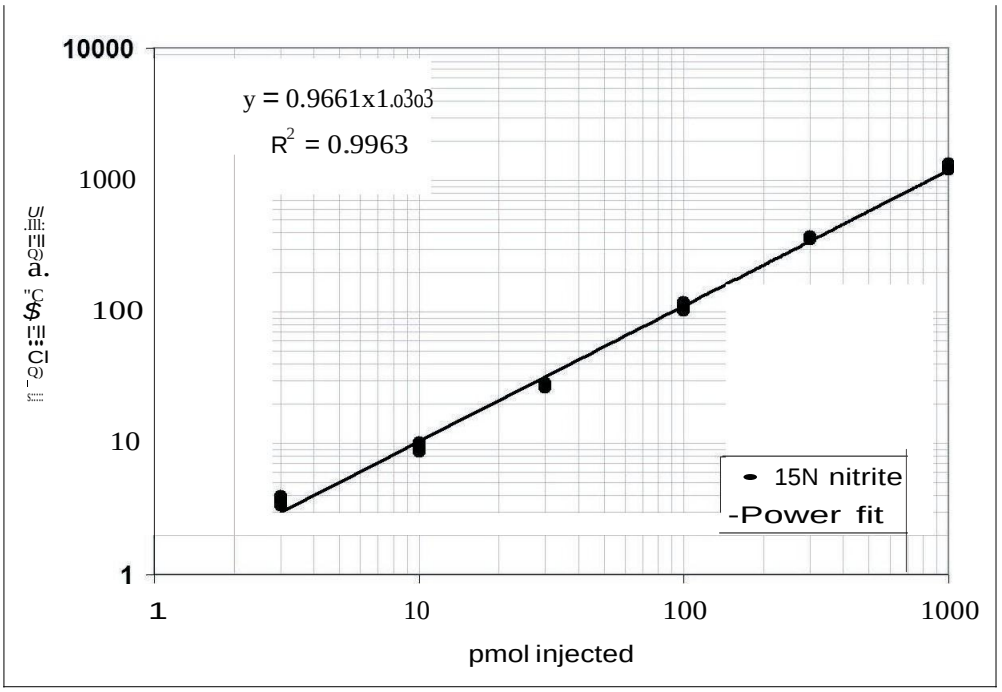

Isotope tracting for NO chemiluminescence assays

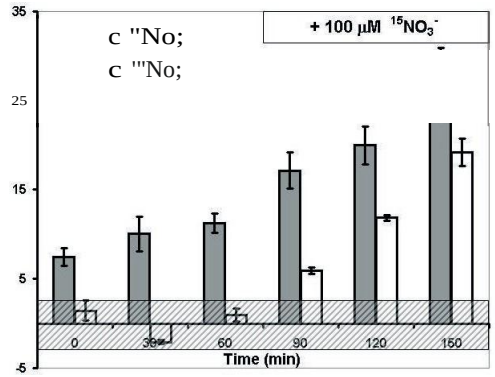

c "No;
c '"No;

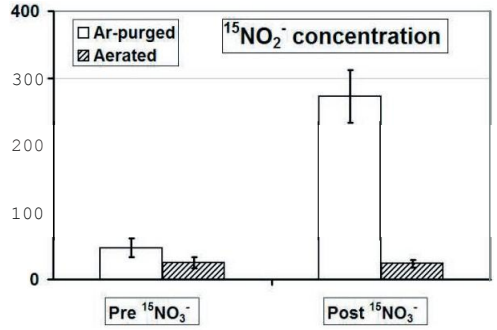

c:
a.
E
O
E
a.